JACS
JOURNAL OF THE AMERICAN CHEMICAL SOCIETY
Communication
Cite This: J. Am. Chem. Soc. 2019, 141, 16232−16236
pubs.acs.org/JACS

Characterization of a Reactive Rh_2 Nitrenoid by Crystalline Matrix Isolation

Anuvab Das,[†] Yu-Sheng Chen,[‡] Joseph H. Reibenspies,[†] and David C. Powers*[,†]

[†]Department of Chemistry, Texas A&M University, College Station, Texas 77843, United States
[‡]ChemMatCARS, University of Chicago c/o APS/ANL, Argonne, Illinois 60439, United States

Supporting Information

ABSTRACT: The fleeting lifetimes of reactive intermediates in C−H functionalization chemistry often prevent their direct characterization. For example, the critical nitrenoid intermediates that mediate Rh_2-catalyzed C−H amination have eluded characterization for more than 40 years. In the absence of structural characterization of these species, methodological development is often computationally guided. Here we report the first X-ray crystal structure of a reactive Rh_2 nitrenoid, enabled by N_2 elimination from an organic azide ligand within a single-crystal matrix. The resulting high-resolution structure displays metrical parameters consistent with a triplet nitrene complex of Rh_2. The demonstration of facile access to reactive metal nitrenoids within a crystalline matrix provides a platform for structural characterization of the transient species at the heart of C−H functionalization.

Unstabilized nitrenes are reactive, high-energy species that feature a hextet electronic configuration at nitrogen (i.e., N−R species).[1] Nitrenes participate in a diverse reaction manifold, including C−H insertion, addition to C−C multiple bonds, and various unimolecular rearrangements, that render these species challenging to utilize as intermediates in selective synthetic chemistry.[2] Synthetic chemists[3] and biologists[4] have advanced selective nitrene-transfer chemistry that is predicated on leveraging the reactivity of transition metal-stabilized nitrenoid intermediates for C−H functionalization and olefin aziridination. In particular, Rh_2 catalysis has emerged as a broadly useful platform in nitrene-transfer catalysis (Figure 1).[5] Critical Rh_2 nitrenoid intermediates have been detected by mass spectrometry[6] and time-resolved spectroscopic methods,[7] but due to their fleeting lifetimes, structural data of these transient species has not been available. Significant questions, such as the preferred electronic configuration of Rh_2 nitrenoids, have not been resolved despite sustained interest.[8]

Unambiguous molecular structure determination can be achieved by X-ray diffraction, but requires chemical samples that are sufficiently kinetically stable to be crystallized. The inherently transient nature of reactive intermediates typically precludes application of X-ray diffraction to the characterization of these species. Two methods have been advanced to gain structural information about reactive intermediates in the condensed phase: (1) structural characterization of synthetic derivatives designed to attenuate the reactivity of the intermediate of interest, for example via introduction of sterically encumbering ligands,[9] and (2) spectroscopic characterization of photogenerated reactive intermediates by cryogenic matrix isolation.[10] We envisioned that photogeneration of reactive intermediates within a crystalline matrix would combine classical matrix isolation with X-ray diffraction and enable structural characterization of these species without synthetic derivatization.[11] Here, we demonstrate the successful application of this strategy to the characterization of a Rh_2 nitrenoid generated by N_2 elimination from a Rh_2 alkylazide complex within a crystalline matrix.

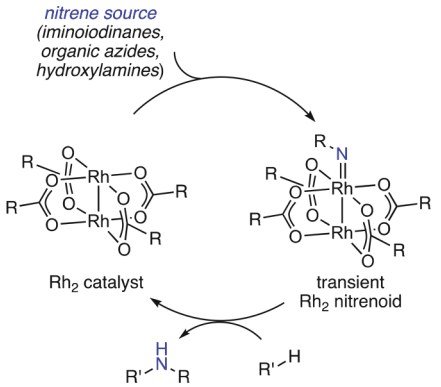

Figure 1. Rh_2-catalyzed nitrene transfer chemistry has emerged as a leading method for introducing nitrogen content in organic molecules. These reactions are proposed to proceed via transient Rh_2 nitrenoids, which have thus far eluded structural characterization.

We targeted characterization of a nitrenoid supported by $Rh_2(esp)_2$ (**1**), in which the Rh_2 core is supported by two chelating bis-carboxylate ligands,[5c,12] because complex **1** has emerged as a particularly effective, and widely utilized, nitrene-transfer catalyst.[5c,e−h] We initiated our studies by exploring the synthesis of Rh_2 complexes with organic azide ligands based on the hypothesis that facile N_2 extrusion would provide access to Rh_2 nitrenoids. Exposure of $Rh_2(esp)_2$ to CH_2Cl_2 solutions of AdN_3 resulted in sequential formation of two Rh_2 azide adducts: $Rh_2(esp)_2(AdN_3)$ (**2a**) and $Rh_2(esp)_2(AdN_3)_2$ (**2b**). Concentration-dependent UV−vis spectra display isosbestic points connecting $Rh_2(esp)_2$ (**1**) and $Rh_2(esp)_2(AdN_3)$ (**2a**) at 0−12 mM $[AdN_3]$ and isosbestic points connecting **2a** and $Rh_2(esp)_2(AdN_3)_2$ (**2b**) at 12−85 mM $[AdN_3]$ implying the

Received: August 21, 2019
Published: September 24, 2019

DOI: 10.1021/jacs.9b09064
J. Am. Chem. Soc. 2019, 141, 16232−16236

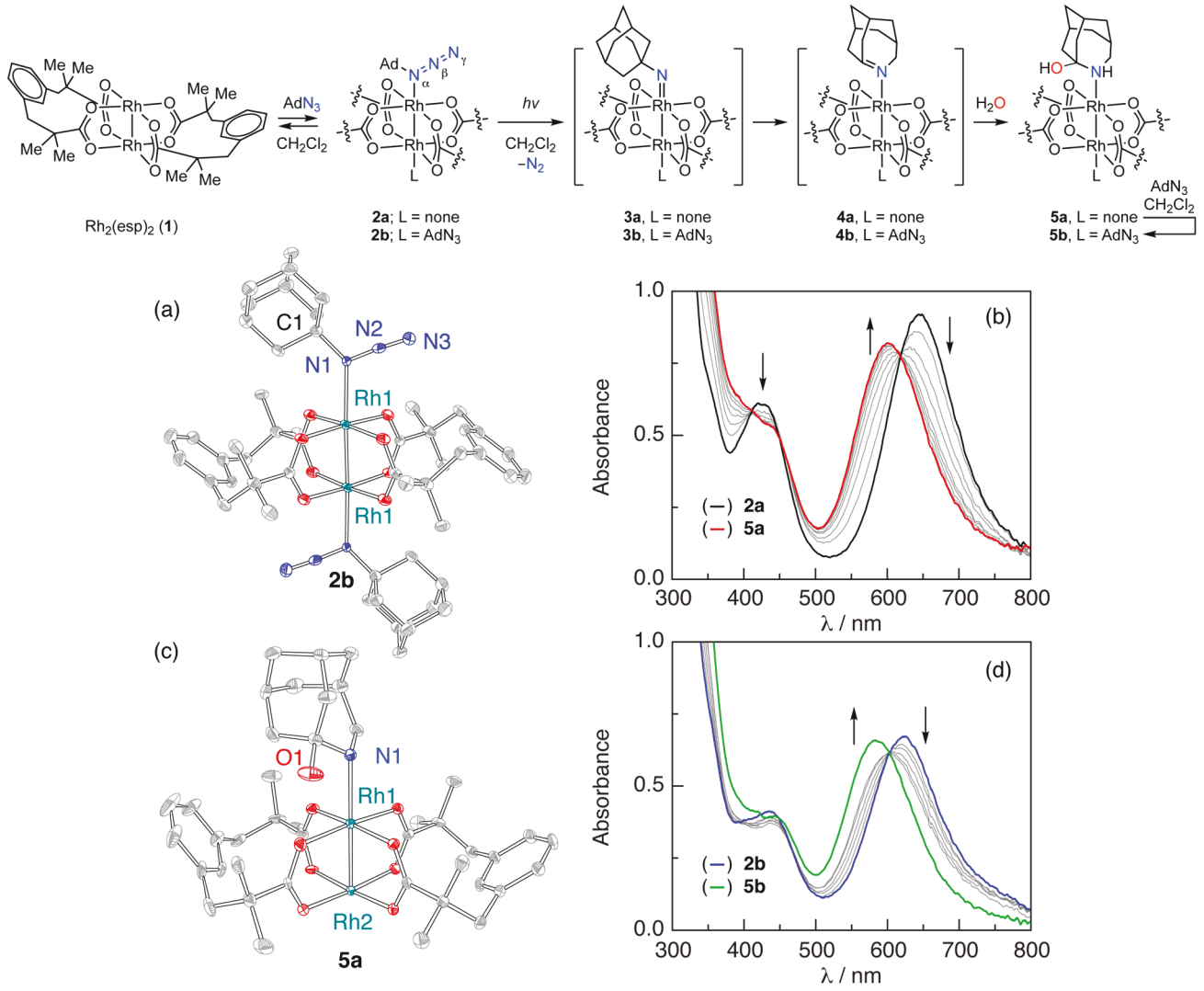

Figure 2. Synthesis and steady-state photochemistry of organoazide complexes of $Rh_2(esp)_2$ (**1**). Treatment of $Rh_2(esp)_2$ (**1**) with AdN_3 results in sequential formation of $Rh_2(esp)_2(AdN_3)$ (**2a**) and $Rh_2(esp)_2(AdN_3)_2$ (**2b**). (a) Thermal ellipsoid plot of **2b** drawn at 50% probability with H atoms and solvent removed for clarity. Rh(1)–Rh(1): 2.3968(8) Å, Rh(1)–N(1): 2.335(3) Å, N(1)–C(1): 1.509(5) Å, N(1)–N(2): 1.254(5) Å, N(2)–N(3): 1.135(5) Å, N(1)–N(2)–N(3): 176.1(4)°. (b) UV–vis spectra collected during the photolysis of Rh_2 complex **2a** in CH_2Cl_2 (335 nm < λ < 610 nm). Isosbestic points are observed at 411, 455, and 618 nm, which indicate the lack of a steady-state intermediate in the conversion of **2a** to **5a**. (c) Thermal ellipsoid plot of **5a** drawn at 50% probability with H atoms and solvent removed for clarity. Selected metrical parameters: Rh(1)–Rh(2): 2.3959(5) Å; Rh(1)–N(1): 2.303(4) Å. (d) UV–vis spectra collected during the photolysis of Rh_2 complex **2b** in CH_2Cl_2 (335 nm < λ < 610 nm). An isosbestic point is observed at 603 nm, which indicates the lack of a steady-state intermediate in the conversion of **2b** to **5b**.

absence of steady-state intermediates in these reactions (Figure S1). Further spectral evolution was not observed upon further addition of AdN_3. Job's analysis confirms that **2a** is a 1:1 adduct of $Rh_2(esp)_2$ and AdN_3 (Figure S2 and Table S1). Rapid exchange of free and bound AdN_3 is evident in the room temperature ^{1}H NMR spectra of **2a** and **2b**. Low-temperature ^{1}H NMR spectroscopy and electrospray ionization mass spectrometry (ESI-MS) support the formulation of **2a** and **2b** as mono- and bis-azide adducts, respectively (Figures S3 and S4). The AdN_3 ligands are weakly bound; titration of a tetrahydrofuran solution of $Rh_2(esp)_2$ with AdN_3 results in no spectral changes, which suggests AdN_3 does not displace bound THF ligands at the apical sites of $Rh_2(esp)_2$.

Single crystals of **2b** were obtained from cooling a CH_2Cl_2 solution of $Rh_2(esp)_2$ and AdN_3. X-ray diffraction analysis revealed the structure depicted in Figure 2a in which two symmetry-equivalent AdN_3 ligands are bound to the Rh_2 core via N(α). Efforts to crystallize **2a** by lowering the AdN_3 loading consistently provided bis-azide adduct **2b** as the exclusive crystallization product, which suggests the preferential crystallization of **2b** over mono-azide adduct **2a**. The Rh–Rh distance in **2b** (2.3968(8) Å) is similar to that previously reported for $Rh_2(esp)_2S_2$ complexes (S = solvent-derived ligands, see Table S2). The N_3 fragment of the AdN_3 ligand is nearly linear (N(1)–N(2)–N(3) = 176.2(4)°), the N(1)–N(2) and N(2)–N(3) distances are similar to those in free AdN_3, and the infrared (IR) spectrum of **2b** displays ν_{N3} at 2120 and 2093 cm^{-1} (Figure S5). These metrics are consistent with AdN_3 binding as a σ-donor with insignificant π-backbonding.[13]

Rh_2 complexes **2a** and **2b** are photoprecursors to Rh_2 nitrenoids. Photolysis of a CH_2Cl_2 solution of **2a** (335 nm < λ < 610 nm) resulted in new spectral features that are accessed via well-anchored isosbestic points at 411, 455, and 618 nm

DOI: 10.1021/jacs.9b09064
J. Am. Chem. Soc. 2019, 141, 16232–16236

(Figure 2b). Crystallization of the photolysis reaction mixture afforded a single crystal of **5a** (Figure 2c). Compound **5a** can be envisioned as arising from C-to-N migration within an adamantyl nitrene ligand to generate a transient 2-azahomoadamant-3-ene ligand and subsequent trapping with adventitious water to give rise to the observed hemiaminal ligand (see Figure S6). The observed structure is consistent both with the known low-temperature rearrangement of adamantyl nitrene and with the electrophilicity of highly strained anti-Bredt imines.[14] The UV−vis spectrum of a CH_2Cl_2 solution of **5a** is well-matched to the UV−vis spectrum obtained following photolysis of **2a** (Figure S7). Similarly, photolysis of complex **2b** (335 nm < λ < 610 nm) proceeds via a well-anchored isosbestic point at 603 nm (Figure 2d). The product of photolysis was assigned as **5b** by comparison of the final UV−vis spectrum obtained from photolysis of **2b** with the spectrum generated by addition of AdN_3 to **5a** (Figure S8).

Matrix-assisted laser desorption−ionization mass spectrometry (MALDI-MS) data provided additional evidence for facile N_2 elimination from **2** (Figure 3). Ablation of a sample of **2a**

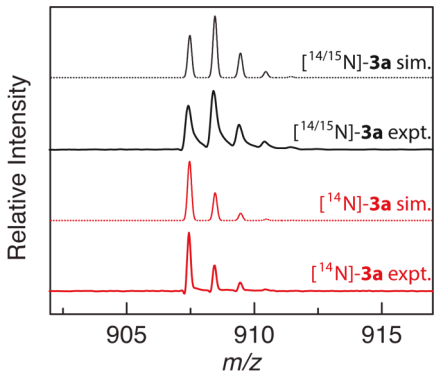

Figure 3. Mass spectrometry evidence for N_2 loss from Rh_2 complexes. MALDI-MS data were acquired for ablation of samples of **2a** and [^{15}N]-**2a**, which indicate the facile loss of N_2 from these complexes to generate $Rh_2(esp)_2(AdN)$ fragments.

produces an ion at m/z = 907.5, which is well matched to the expected mass of $Rh_2(esp)_2(AdN)^+$ (calc = 907.2) and displays the expected isotopic distribution. Ablation of a sample of [^{15}N]-**2a**, prepared from monolabeled [^{15}N]-AdN_3, provided the expected +1 m/z (m/z = 908.4 (expt); 908.2 (calc)) and displays the isotope pattern expected for a 1:1 mixture of **2a** and [^{15}N]-**2a**, which results from incorporation of 50% ^{15}N at each of N(α) and N(γ) in [^{15}N]-AdN_3. *In situ* IR analysis of both photolyzed or thermolyzed KBr pellets of **2b** further indicate facile N_2 loss from **2b** (Figures S9 and S10).

We hypothesized that low-temperature N_2 extrusion from **2b** within a single crystal habit would enable direct structural characterization of nitrenoid **3b**. To this end, we examined the *in situ* structural evolution of a single-crystal of **2b** by X-ray diffraction during irradiation with a 365 nm light source. Data was collected at 100 K with 50 keV synchrotron radiation.[15] Solid-state reaction progress was monitored by free refinement of the nitrogen occupancies, which indicate that while the occupancy of N(α) was unchanged with time, the occupancy of N(β) decreased. Concurrently, the space group was observed to transition from monoclinic $P2_1/c$ to $P2_1/n$.[16] Refinement of the resulting data indicated elimination of a molecule of N_2 to afford Rh_2 nitrenoid **3b**·N_2 (Figure 4). Upon N_2 extrusion, Rh(1)−N(1B) (i.e., the nitrenoid linkage)

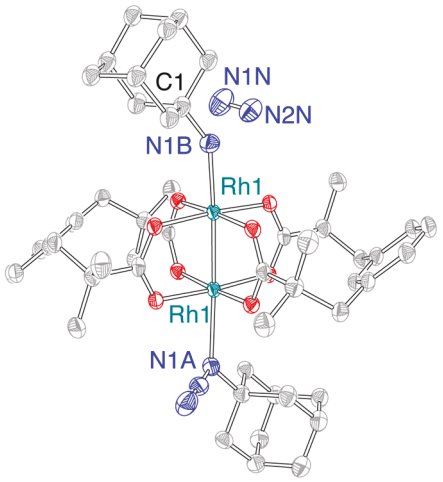

	3b expt.	^{3}[**3b**] comp.	^{1}[**3b**] comp.
Rh(1)–N(1B) / Å	2.12(2)	2.094	1.924
Rh(1)–N(1A) / Å	2.346(4)	2.408	2.534
Rh(1)–Rh(1) / Å	2.3903(4)	2.438	2.465
Rh(1)–N(1B)–C(1) / °	147.2(9)	136.9	126.8

Figure 4. Solid-state structure of reactive Rh_2 nitrenoid 3b. Thermal ellipsoid plot of **3b**·N_2 generated by solid-state N_2 elimination from **2b**. Ellipsoids are drawn at 50% probability. H atoms and solvent are removed for clarity. The structure illustrated here results from refinement of a data set collected at 46% conversion; higher conversions can be achieved but at the expense of crystallinity (see Supporting Information). Comparison of the bond metrics derived from the X-ray structure with those computed for ^{3}[**3b**] and ^{1}[**3b**] indicate excellent agreement with the triplet electronic configuration.

contracts from 2.335(3) Å (**2b**) to 2.12(1) Å (**3b**). Concurrent with N_2 extrusion and Rh(1)−N(1B) contraction, significant contraction of N(1B)−C(1) (i.e., the N−C bond in the adamantyl nitrene fragment) is also observed from 1.509(5) Å (**2b**) to 1.41(2) Å (**3b**). The conversion of **2b** to **3b** is also accompanied by a significant expansion of the Rh(1)−N(B)−C(1) angle from 129.1° to 147.2°. No substantial changes in the C−C distances of the adamantyl fragment were observed, and both Rh(1)−Rh(1) (2.3968(8) Å (**2b**); 2.3903(4) Å (**3b**)) and Rh(1)−N(1A) (i.e., the Rh−N(Ad)N_2 linkage; 2.335(3) (**2b**); 2.346(4) Å (**3b**)) are essentially unchanged. The Rh centers in **3b**·N_2 are symmetry equivalent, and thus following loss of N_2 the AdN_3 and AdN ligands of **3b** are compositionally disordered (i.e., 50% occupancy of each AdN and AdN_3 on each of the Rh centers). Solid-state conversion of up to 70% are well accommodated within the single crystal. Attempts to achieve higher conversions or to promote loss of a second equivalent of N_2 to generate a bis-nitrenoid by prolonged irradiation were unsuccessful due to loss of crystallinity (see Supporting Information for details).

Density functional theory (DFT) optimization of the geometry of **3b** has been pursued both as a singlet and as a triplet electronic configuration (i.e., ^{1}[**3b**] and ^{3}[**3b**]; M06 functional, LANL2DZ basis set for Rh, 6-31G** for other atoms).[17] The calculated Rh(1)−Rh(1), Rh(1)−N(1A), Rh(1)−N(1B), and N(1B)−C(1) distances and Rh(1)−N(1B)−C(1) angle for ^{3}[**3b**] are in excellent agreement with the experimentally defined parameters (Figure 4). In contrast, the optimized structure of ^{1}[**3b**] substantially underestimates both the Rh(1)−N(1B) distance (1.924 Å (calc); 2.12(2) Å

DOI: 10.1021/jacs.9b09064
J. Am. Chem. Soc. 2019, 141, 16232−16236

(expt)) and Rh(1)−N(1B)−C(1) angle (126.8° (calc); 147.2° (expt)) and substantially overestimates the Rh(1)−N(1A) distance (2.534 Å (calc); 2.346(4) Å (expt)). The observation of ^{3}[**3b**] is consistent with the relative stabilities computed for ^{1}[**3b**] and ^{3}[**3b**]; the singlet structure is calculated to be 5.5 kcal/mol above the triplet.[18] One might expect that a singlet nitrene would be best stabilized in a bent geometry that maximizes back-bonding into a vacant p-orbital. We speculate that the observed linearization of the nitrenoid fragment in **3b** enables the triplet nitrene to be stabilized by two half-order π-bonds generated by overlap of filled Rh−Rh π^* orbitals with partially occupied *N*-centered orbitals.[17]

In closing, the characterization of nitrenoid **3b** reported here establishes the electronic and three-dimensional structures of this critical intermediate. Typically, structural characterization of the transient intermediates involved in the intimate bond-forming and -breaking processes during catalysis is not possible, and thus investigations of reaction mechanisms often rely on computational characterization of reactive intermediates using methods optimized for isolated catalyst intermediates. We anticipate that direct characterization of reactive nitrenoid intermediates will inform rational development of C−H amination chemistry. Further, the demonstration of crystalline matrix confinement as a platform for the structural characterization of reactive intermediates raises the tantalizing possibility that proper design of photoactive molecular precursors may represent a general strategy to directly characterize reactive species generated by elimination of small molecules within crystalline samples.

■ ASSOCIATED CONTENT

Supporting Information

The Supporting Information is available free of charge on the ACS Publications website at DOI: 10.1021/jacs.9b09064.

Experimental procedures, spectroscopic and crystallographic data, and coordinates of optimized structures (PDF)

X-ray crystallographic data for **2b**, **3b**·N_2, **5a**, and **S1** (CIF)

■ AUTHOR INFORMATION

Corresponding Author

*david.powers@chem.tamu.edu

ORCID

Anuvab Das: 0000-0002-9344-4414

David C. Powers: 0000-0003-3717-2001

Notes

The authors declare no competing financial interest.

■ ACKNOWLEDGMENTS

The authors acknowledge the U.S. Department of Energy (DOE), Office of Science, Office of Basic Energy Sciences, Catalysis Program under Award Number DE-SC0018977 and the Welch Foundation (A-1907) for financial support. X-ray diffraction data of **2b** and **3b**·N_2 were collected at ChemMatCARS Sector 15 housed at the Advanced Photon Source (APS) at Argonne National Laboratory (ANL), which is supported by the Divisions of Chemistry (CHE) and Materials Research (DMR), National Science Foundation, under grant number NSF/CHE-1834750. Use of the APS, an Office of Science User Facility operated for the U.S. DOE Office of Science by ANL, was supported by the U.S. DOE under Contract No. DE-AC02-06CH11357.

■ REFERENCES

(1) Wentrup, C. Carbenes and Nitrenes: Recent Developments in Fundamental Chemistry. *Angew. Chem., Int. Ed.* **2018**, *57*, 11508−11521.

(2) Dequirez, G.; Pons, V.; Dauban, P. Nitrene Chemistry in Organic Synthesis: Still in Its Infancy? *Angew. Chem., Int. Ed.* **2012**, *51*, 7384−7395.

(3) (a) Svastits, E. W.; Dawson, J. H.; Breslow, R.; Gellman, S. H. Functionalized Nitrogen Atom Transfer Catalyzed by Cytochrome P-450. *J. Am. Chem. Soc.* **1985**, *107*, 6427−6428. (b) Davies, H. M. L.; Manning, J. R. Catalytic C−H Functionalization by Metal Carbenoid and Nitrenoid Insertion. *Nature* **2008**, *451*, 417−424. (c) Roizen, J. L.; Harvey, M. E.; Du Bois, J. Metal-Catalyzed Nitrogen-Atom Transfer Methods for the Oxidation of Aliphatic C−H Bonds. *Acc. Chem. Res.* **2012**, *45*, 911−922. (d) Gephart, R. T., III; Warren, T. H. Copper-Catalyzed sp^3 C−H Amination. *Organometallics* **2012**, *31*, 7728−7752. (e) Alderson, J. M.; Corbin, J. R.; Schomaker, J. M. Tunable, Chemo- and Site-Selective Nitrene Transfer Reactions through the Rational Design of Silver(I) Catalysts. *Acc. Chem. Res.* **2017**, *50*, 2147−2158. (f) Park, Y.; Kim, Y.; Chang, S. Transition Metal-Catalyzed C−H Amination: Scope, Mechanism, and Applications. *Chem. Rev.* **2017**, *117*, 9247−9301. (g) Singh, R.; Mukherjee, A. Metalloporphyrin Catalyzed C−H Amination. *ACS Catal.* **2019**, *9*, 3604−3617.

(4) (a) Brandenberg, O. F.; Fasan, R.; Arnold, F. H. Exploiting and engineering hemoproteins for abiological carbene and nitrene transfer reactions. *Curr. Opin. Biotechnol.* **2017**, *47*, 102−111. (b) Prier, C.; Zhang, R. K.; Buller, A. R.; Brinkmann-Chen, S.; Arnold, F. H. Enantioselective, intermolecular benzylic C−H amination catalyzed by an engineered iron-haem enzyme. *Nat. Chem.* **2017**, *9*, 629−634. (c) Cho, I.; Jia, Z.-J.; Arnold, F. H. Genetically Tunable Enzymatic C−H Amidation for Lactam Synthesis. *Science* **2019**, *364*, 575−578.

(5) (a) Nageli, I.; Baud, C.; Bernardinelli, G.; Jacquier, Y.; Moraon, M.; Mullet, P. Rhodium(II)-Catalyzed CH Insertions with {[(4-Nitrophenyl)sulfonyl]imino}phenyl-λ^3-iodane. *Helv. Chim. Acta* **1997**, *80*, 1087−1105. (b) Espino, C. G.; Wehn, P. M.; Chow, J.; Du Bois, J. Synthesis of 1,3−Difunctionalized Amine Derivatives through Selective C−H Bond Oxidation. *J. Am. Chem. Soc.* **2001**, *123*, 6935−6936. (c) Espino, C. G.; Fiori, K. W.; Kim, M.; Du Bois, J. Expanding the Scope of C−H Amination through Catalyst Design. *J. Am. Chem. Soc.* **2004**, *126*, 15378−15379. (d) Stokes, B. J.; Dong, H.; Leslie, B. E.; Pumphrey, A. L.; Driver, T. G. Intramolecular C−H Amination Reactions: Exploitation of the Rh_2(II)-Catalyzed Decomposition of Azidoacrylates. *J. Am. Chem. Soc.* **2007**, *129*, 7500−7501. (e) Nguyen, Q.; Sun, K.; Driver, T. G. Rh_2(II)-Catalyzed Intramolecular Aliphatic C−H Bond Amination Reactions using Aryl Azides as the *N*-Atom Source. *J. Am. Chem. Soc.* **2012**, *134*, 7262−7265. (f) Jat, J. L.; Paudyal, M. P.; Gao, H.; Xu, Q.-L.; Yousufuddin, M.; Devarajan, D.; Ess, D. H.; Kürti, L.; Falck, J. R. Direct and Stereospecific Synthesis of Unprotected N−H and N−Me Aziridines from Olefins. *Science* **2014**, *343*, 61−65. (g) Paudyal, M. P.; Adebesin, A. M.; Burt, S. R.; Ess, D. H.; Ma, Z.; Kürti, L.; Falck, J. R. Dirhodium-catalyzed C-H arene amination using hydroxylamines. *Science* **2016**, *353*, 1144−1147. (h) Chiappini, N. D.; Mack, J. B. C.; Du Bois, J. Intermolecular C(sp^3)−H Amination of Complex Molecules. *Angew. Chem., Int. Ed.* **2018**, *57*, 4956−4959.

(6) Perry, R. H.; Cahill, T. J., III; Roizen, J. L.; Du Bois, J.; Zare, R. N. Capturing fleeting intermediates in a catalytic C−H amination reaction cycle. *Proc. Natl. Acad. Sci. U. S. A.* **2012**, *109*, 18295−18299.

(7) Das, A.; Maher, A. G.; Telser, J.; Powers, D. C. Observation of a Photogenerated Rh_2 Nitrenoid Intermediate in C−H Amination. *J. Am. Chem. Soc.* **2018**, *140*, 10412−10415.

(8) (a) Harrison, J. G.; Gutierrez, O.; Jana, N.; Driver, T. G.; Tantillo, D. J. Mechanism of Rh_2(II,II)-Catalyzed Indole Formation: The Catalyst Does Not Control Selectivity. *J. Am. Chem. Soc.* **2016**, *138*, 487−490. (b) Varela-Álvarez, A.; Yang, T.; Jennings, H.;

DOI: 10.1021/jacs.9b09064
J. Am. Chem. Soc. 2019, 141, 16232−16236

Kornecki, K. P.; Macmillan, S. N.; Lancaster, K. M.; Mack, J. B. C.; Du Bois, J.; Berry, J. F.; Musaev, D. G. Rh_2(II,III) Catalysts with Chelating Carboxylate and Carboxamidate Supports: Electronic Structure and Nitrene Transfer Reactivity. *J. Am. Chem. Soc.* **2016**, *138*, 2327−2341. (c) Wang, J.; Zhao, C.; Weng, Y.; Xu, H. Insight into the mechanism and site-selectivity of $Rh_2^{II,II}(esp)_2$-catalyzed intermolecular C−H amination. *Catal. Sci. Technol.* **2016**, *6*, 5292−5303.

(9) For examples in the context of reactive metal nitrenoid fragments, see: (a) Shay, D. T.; Yap, G. P. A.; Zakharov, L. N.; Rheingold, A. L.; Theopold, K. H. Intramolecular C−H Activation by an Open-Shell Cobalt(III) Imido Complex. *Angew. Chem., Int. Ed.* **2005**, *44*, 1508−1510. (b) Laskowski, C. A.; Miller, A. J. M.; Hillhouse, G. L.; Cundari, T. R. A Two-Coordinate Nickel Imido Complex that Effects C−H Amination. *J. Am. Chem. Soc.* **2011**, *133*, 771−773. (c) Iovan, D. A.; Betley, T. A. Characterization of Iron-Imido Species Relevant for *N*-Group Transfer Chemistry. *J. Am. Chem. Soc.* **2016**, *138*, 1983−1993. (d) Bakhoda, A.; Jiang, Q.; Bertke, J. A.; Cundari, T. R.; Warren, T. H. Elusive Terminal Copper Arylnitrene Intermediates. *Angew. Chem., Int. Ed.* **2017**, *56*, 6426−6430.

(10) Downs, A. J.; Greene, T. M. Coming to Grips with Reactive Intermediates. *Adv. Inorg. Chem.* **1998**, *46*, 101−171.

(11) Das, A.; Reibenspies, J. H.; Chen, Y.-S.; Powers, D. C. Direct Characterization of a Reactive Lattice-Confined Ru_2 Nitride by Photocrystallography. *J. Am. Chem. Soc.* **2017**, *139*, 2912−2915.

(12) The esp ligand is derived from $\alpha,\alpha,\alpha',\alpha'$-tetramethyl-1,3-benzenedipropionic acid.

(13) (a) Dias, H. V. R.; Polach, S. A.; Goh, S.-K.; Archibong, E. F.; Marynick, D. S. Copper and silver complexes containing organic azide ligands: syntheses, structures, and theoretical investigation of $[HB(3,5\text{-}(CF_3)_2Pz)_3]$CuNNN(1-Ad) and $[HB(3,5\text{-}(CF_3)_2Pz)_3]$AgN-(1-Ad)NN (where Pz = Pyrazolyl and 1-Ad = 1-Adamantyl). *Inorg. Chem.* **2000**, *39*, 3894−3901. (b) Seok, W. K.; Klapötke, T. M. Inorganic and Transition Metal Azides. *Bull. Korean Chem. Soc.* **2010**, *31*, 781−788.

(14) Dunkin, I. R.; Shields, C. J.; Quast, H.; Seiferling, B. The Photolysis of 1-Azido-4-Methylbicyclo[2.2.2]octane and 1-Azidoadamantane in Low-Temperature Matrices. *Tetrahedron Lett.* **1983**, *24*, 3887−3890.

(15) Loss of N_2 from **2b** to generate **3b** could be stimulated both by irradiation with 365 nm light and also by prolonged exposure to synchrotron radiation. In addition to the 50 keV radiation used to acquire the data presented above, we have examined the structure of **2b** as a function of time with both 50 and 37.5 keV radiation without 365 nm irradiation and in both cases observed N_2 loss to generate **3b**·N_2 loss was stimulated. The structure generated by photochemically promoted N_2 loss is identical to that promoted by X-ray-stimulated N_2 loss. The X-ray-stimulated loss of N_2 is similar to observations made in protein crystallography regarding the cleavage of weak bonds upon extended irradiation as a mechanism to dissipate incipient X-ray energy. See: Garman, E. Radiation damage in macromolecular crystallography: what is it and why should we care? *Acta Crystallogr., Sect. D: Biol. Crystallogr.* **2010**, *66*, 339−351.

(16) The formation of **3b**·N_2 results in the structure evolution from $P2_1/c$ to $P2_1/n$, with only minor changes in the unit cell parameters [**2b**: a = 10.8913(10) Å, b = 14.274(1) Å, c = 18.732(2) Å, β = 105.847(1)°, V = 2801.7(4) Å^3; **3b**·N_2: a = 11.030(2) Å, b = 14.251(2) Å, c = 18.763(3) Å, β = 107.025(2)°, V = 2820.2(8) Å^3]. This is not a transformation of the monoclinic standard space group $P2_1/c$ to the nonstandard space group $P2_1/n$ [matrix (1 0 1/0 1 0/ −1 0 0), new cell: 18.924, 14.275, 10.891, 107.77].

(17) For these calculations, adamantyl groups were truncated as *tert*-butyl groups. The described computational method has previously been utilized to evaluate the structures of Rh_2 nitrenoids: Varela-Alvarez, A.; Haines, B. E.; Musaev, D. G. Key mechanistic insights into the intramolecular C−H bond amination and double bond aziridination in sulfamate esters catalyzed by dirhodium tetracarboxylate complexes. *J. Organomet. Chem.* **2018**, *867*, 183−192. Computations pursued using the BP86 functional in combination with the TZVP basis set for Rh and 6-31G** for other atoms (ref 8b) are detailed in the Supporting Information.

(18) Similarly, ^{3}[**3a**] is computed to be 6.9 kcal/mol lower in energy than ^{1}[**3a**]. See Supporting Information for details and for discussion of the impact of the apical ligand on the structures of Rh_2 nitrenoids.

DOI: 10.1021/jacs.9b09064
J. Am. Chem. Soc. 2019, 141, 16232−16236